Short Communication

The excellent photocatalytic performances of silver doped ZnO nanoparticles for hydrogen evolution

Irshad Ahmad[1,2] · Ejaz Ahmed[1] · Mukhtar Ahmad[1]

© Springer Nature Switzerland AG 2019

Abstract
Ag based ZnO photocatalyst materials were prepared by facile, quick and inexpensive combustion method followed by calcinations at 700 °C for 3 h. The resulted nanoparticles were characterized using XRD, UV–Vis DRS, SEM, BET, FTIR, XPS, EDX and PL spectroscopy. The XRD analysis of silver doped ZnO (SZO) nanoparticles confirmed hexagonal wurtzite structure of ZnO with minimum crystal size about 19 nm. The doping of Ag in ZnO crystal lattice successfully suppressed the crystal growth of ZnO nanoparticles evidenced by XRD results. The DRS and PL spectra studies revealed that Ag doped ZnO nanoparticles showed absorption in visible light region and charge recombination was efficiently suppressed respectively. The DRS spectra analysis indicated that photon energy band gap Eg for SZO nanoparticles were in the range of 3.27–3.33 eV and reduced with increase in Ag doping. As a novel photocatalyst, the photocatalytic activity for hydrogen evolution was tested by water splitting using ethanol as sacrificial agent under solar light irradiation. The optimal hydrogen evolution rate 805 µmol h^{-1} g^{-1} was shown by 6% SZO photocatalyst. This was nearly 54 times higher hydrogen evolution rate as compared to pure ZnO. The improved photocatalytic activity was attributed to small particle size, plasmon band, charge separation and increased surface area. This report clearly revealed the benefit of using Ag doped ZnO catalyst for higher photocatalytic hydrogen generation.

Keywords ZnO · Combustion · Silver · FTIR · UV–Vis DRS · Hydrogen evolution

1 Introduction

Hydrogen energy is at the top priority of any nation's obligations and goals when discussing the clean and inexpensive energy agenda. Hydrogen energy promises a redly accessible source, harmless emissions, efficient (large energy per mass of fuel), non-toxic (a scarcity among frequent used fuel sources), more dominant (accomplished more in less) and a promising potential candidate. In spite of the fact that hydrogen is frequently and abundantly present everywhere, but never found alone and required to be separated from other species. Unlikely to fossil fuels that are easy to store and transport, hydrogen requires economy challenges and infrastructures for transfer as well as for commercial and industrial use. At last, mostly industrial methods for separating hydrogen still required the application of fossil fuels; it is ironical for that reducing our dependence on the non renewable sources we should depend on them.

Oxidation of hydrocarbons is reputed for such methods [1], but it generates CO_2 and consumes sufficient energy. A very facile process to achieve hydrogen energy is through electrolysis [2]. In this water is exposed to an electric current, which will split water into H_2 and O_2. The apparent drawback is the requirement for an extensive transport of energy. H_2 can also be achieved from biomass gasification

Irshad Ahmad, Ejaz Ahmed, Mukhtar Ahmad have contribute equally in this manuscript.

✉ Irshad Ahmad, i3334405658@gmail.com | [1]Department of Physics, Bahauddin Zakariya University, Multan 60800, Pakistan. [2]Paradise Medical Store Near Abbas Plaza, Multan, Punjab, Pakistan.

SN Applied Sciences (2019) 1:327 | https://doi.org/10.1007/s42452-019-0331-9

Received: 30 January 2019 / Accepted: 3 March 2019 / Published online: 9 March 2019

[3–6], but application is restricted by the economical feasibility of the mechanism.

Application of light irradiation process to already existing processes can be sufficiently improved, resulting in H_2 evolution from renewable sources. Naturally this requires the application of light energy to become really free of non-renewable sources [7, 8]. The required alternate hydrogen production sources believed to be photocatalytic water splitting and oxidation of hydrocarbons (photocatalytic reforming of biomass) [9–11]. The later is useful since H_2 is generated with photocatalytic degradation of organic molecules existing in water at mild conditions, also participating to purification of commercial water. This process could attract even more attention, if natural renewable sources (such as solar energy, largely rich in South American and European regions) are used.

Titanium dioxide (TiO_2) had been widely used in photo induced processes [12, 13]. The extensive use of this salt had increased the search for alternate attractive photocatalyst with enhanced properties [14]. ZnO is a wide band gap semiconductor photocatalyst similar to that of titanium dioxide (TiO_2). In addition ZnO is inexpensive and contains exceptional morphologic versatility [15]. ZnO materials can be synthesized with different shapes like nanoparticles, Nanotubes, nanotetra pods, nanospheres, nanorods, nanoflowers etc. [16–18]. These synthesized materials are normally designated as tunable band gap semiconductors and can absorb in UV region of solar spectrum. The scientific community attempted to modify the energy band gap of TiO_2 and ZnO due to their restricted activity under visible light irradiation, and this band gap modification will increase solar light absorption in visible range. Structural and morphological modifications were made to enable these materials as efficient photocatalysts. The application of TiO_2 hybrids including carbons like carbon fibers, carbon Nanotubes, activated carbon, graphene etc. had been reported as efficient technique to increase the semiconductor photocatalytic activity under UV and visible light irradiation [19–30]. Dye photo-sensitization variations had also been reported. The photocatalytic activity of both TiO_2 and ZnO has been enhanced with metal doping like Ag [31–35]. The silver had been selected for doping purpose due to its band fluctuation ability [36]. Silver is a noble metal which shows several properties such as no photo-corrosion, anchored on surface and surface Plasmon band in visible range [37, 38]. Although, Ag doped TiO_2 photocatalyst had been reported in the presence of ethanol as sacrificial agent [37, 38], but Ag doped ZnO photocatalyst had not been reported as photocatalyst for hydrogen generation. In this work, we reported Ag doped ZnO photocatalyst for photocatalytic hydrogen production which was synthesized by facile, quick, time saving and inexpensive combustion method. Moreover, synthesized photocatalysts had showed higher photocatalytic activity for hydrogen generation. The synthesized photocatalysts were tested for photocatalytic hydrogen evolution in the presence of water–ethanol solution under solar light irradiation.

2 Experimental

2.1 Synthesis of ZnO materials

Combustion method was used to synthesize ZnO and silver doped ZnO nanoparticles $Ag_xZn_{1-x}O$ (x = 0, 1%, 2%, 4%, 6%, 8%) using Zinc Nitrate Hexahydrate [$Zn(NO_3)_2{\cdot}6(H_2O)$], silver nitrate ($AgNO_3$) and glycine (NH_2CH_2COOH). All reagents were bought from Merck Pakistan with 99.90% purity. Zinc Nitrate Hexahydrate and silver nitrate were used as oxidant while Glycine was used as fuel for combustion process. In this study fuel to oxidant molar ratio (Ψ) was taken as 1.7 due to its optimal previous results [15]. The required amount of all Ag doped ZnO nanoparticles as said above $Ag_xZn_{1-x}O$ were taken in beakers. The zinc nitrate Hexahydrate being hygroscopic absorbed moisture and turned into transparent slurry. The slurry was heated at hot plate with constant stirring to make homogeneous solution. The process of mixing continued for 1 h and then temperature of solution was increased to 280 °C with continuous stirring on hot plate. The color of the solution changed from white to red, red to yellow and yellow to black at high temperature of 280 °C. The solution was swallowed into foam like black gel and burst with evolution of heat and large amount of non-toxic gases and result in dry, loose and voluminous black nano powders with high porosity. The heat treatment was applied at 700 °C for 3 h to absorb any remained moisture in nano powders, which changed the color of nanoparticles to white. The ZnO doped with 1, 2, 4, 6 and 8% mol of silver were labeled as samples 1%SZO, 2%SZO, 4%SZO, 6%SZO, and 8%SZO respectively.

2.2 Characterization of ZnO and Ag–ZnO photocatalysts

The crystal structure of the synthesized nanoparticles was studied by using Panalytical Empyrean X-Ray diffractometer using Cu-Kα radiation (λ = 1.5406 Å) with 2θ scanning range 20°–80° at step width of 0.02°. The particle size was measured by Scherer formula

$$D = k\lambda/\beta\cos\theta$$

Here D is particle size, k is shape factor with value 0.9, λ = 0.15406 nm is wavelength of Cu-Kα radiation source, β is full width at half maximum (FWHM) measured in radians

and θ is diffraction angle. The scanning electron microscope (SEM), Hitachi S-4800 was applied to observe the morphology of nanoparticles. The compositional analysis of the synthesized nanoparticles was studied by energy dispersive X-ray spectroscopy. The optical characteristics of the synthesized samples were recorded using a PerkinElmer-lambda 5 UV–visible spectrophotometer and energy band gaps were measured by the Kubelka–Munk function. PL spectra were recorded at room temperature equipped with Crylas CW-276 nm Laser as an exciton source. The emission was recorded by a CCD camera coupled with grating mono-chromator laser and power was maintained in 2 mW. FTIR spectra were measured by JASCO-MFT 2000 apparatus. The interval of operating parameters was 4000–500 cm^{-1} with 32 scans along with mirror velocity of 0.6139 cm/s. Brunauer–Emmett–Teller specific surface area was measured by Gemini-2375, Shimadzu.

2.3 Photo activity

The photocatalytic hydrogen production was operated in doubled walls quartz photo-chemical reactor. A mixture containing 10 mg mass of the synthesized sample and 12 mL of ethanol solution with volume ratio (ethanol: water) of 1:5 was obtained through constant magnetic stirring. Continuous water circulating through the photochemical reactor was arranged with the help of thermostatic bath to maintain the room temperature. Argon (Ar) bubbling by deaerator was carried out for 30 min to wipe out any air traces before irradiation. A 300 W mercury xenon (Hg–Xe) lamp of PerkinElmer- CarMax PE-300 was used as irradiation source. Agilent 8620-GC chromatograph coupled with TCD with the help of Porapak Q (90/100 mesh) column was used to measure room temperature produced gases during experiments with the help of gas chromatograph, using Ar as carrier wave. A gas-tight syringe with optimum volume of 80 mL was used to measure the amount of gas evolved at time interval of 30 min. To test the reproducibility of the hydrogen evolution activity, each photocatalyst was tested three times.

3 Results and discussions

3.1 Photocatalysts characterization

The X-ray diffraction pattern of as-synthesized ZnO and SZO photocatalysts as shown in Fig. 1 reveals typical ZnO hexagonal wurtzite phase (JCPDS No 89-0510). XRD pattern clearly showed crystalline diffraction peaks at 2θ values 31.59 °C, 34.380, 36.240, 47.640, 56.650, 62.960, 66.260, 68.070, 69.260 and 77.370 correspond to (100), (002), (101), (102), (110), (103), (200), (112), (201) and (202) peaks respectively [39]. Two additional peaks observed at 2θ values of 38.40°, 44.35° (JCPDS No 87-0720) correspond to silver (111) and (200) planes, due to elemental growth of silver in ZnO lattice [40]. The silver peak observed at 2θ value of 44.35° was weak for 1%SZO and 2%SZO samples and became clearly visible at higher doping of Ag in ZnO while (111) silver peak was visible at lower Ag doping and became more sharp at higher Ag doping in ZnO lattice. The particle size estimated by Scherer formula was decreased with Ag doping for SZO nanoparticles [41] as shown in Table 1. Particle size is very important for photocatalytic activity. It was observed that intensity of major peaks was reduced with Ag doping, attributed to decrease in crystallinity due to generation of defects caused by silver doping in ZnO [42]. There was no indication for presence of AgO and Ag_2O phase at 2θ value 32.8°. Hence XRD pattern verified the absence of silver oxide phase and presence of metallic silver phase [43]. It was concluded that Ag atoms were not loaded into ZnO lattice but rather grown on the

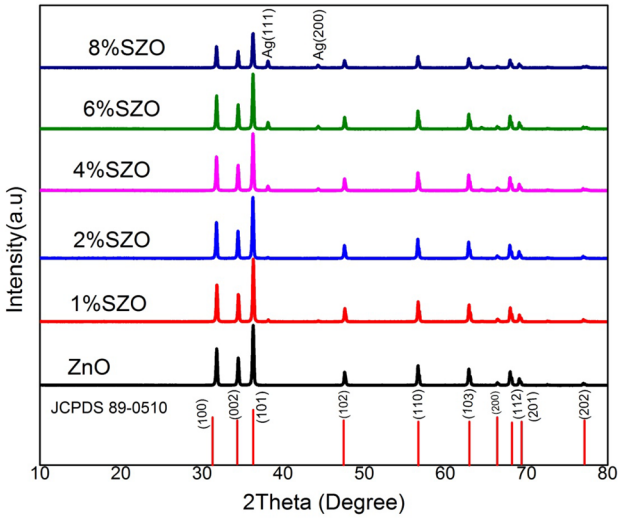

Fig. 1 Exhibits XRD pattern of ZnO and SZO photocatalysts

Table 1 Shows particle size, surface area and hydrogen evolution rate

Photocatalyst composition	Particle size (nm)	Surface area ($m^2\ g^{-1}$)	Hydrogen evolution rate ($\mu mol\ h^{-1}\ g^{-1}$)	Energy band gap (eV)
ZnO	40.2	18	15	3.33
1%SZO	33.5	20	256	3.32
2%SZO	24.0	26	478	3.31
4%SZO	23.0	28	696	3.30
6%SZO	19.0	30	805	3.27
8%SZO	19.6	31	713	3.29

surface of ZnO [44]. Similar observations were reported in earlier studies [42, 45].

If Ag was substituted for Zn^{+2} then corresponding peak shift should be observed in XRD pattern or presence of peak corresponding to AgO or Ag_2O phase in XRD pattern. Since XRD pattern showed no such peak shift, suggested that there exist no positional variation of peaks. XRD pattern indicated broadening of peaks due to presence of clusters. Similar observations had been reported for ZnO [42, 46]. The absence of AgO or Ag_2O phase as mentioned above, showed the absence of Ag substitution in ZnO lattice [47]. Previous reports told that Lupan et al. [48] had assigned analogous peaks both for AgO and Ag_2O, though there was no evidence for the presence of these peaks in our case. Also peak shift had been reported in their work while we did not observe such peak shifts, hence our samples contained only silver. To conclude, SZO photocatalysts maintained hexagonal wurtzite structure, while particle size and intensity was reduced with Ag doping into ZnO lattice. Thus crystallinity was decreased due to creation of defects with Ag doping in ZnO system. Further XRD pattern did shown any peak shift with Ag doping, indicating that Ag atoms were grown on the surface of ZnO and there was no incorporation of Ag due to substitution or interstitial effects. The low particle size will be suitbale for maximum photocatalytic activity.

3.2 UV–Vis diffuse reflectance spectroscopy analysis

DRS study was used to confirm the presence of metallic Ag into ZnO lattice. The DRS spectra showed that there was no observed structural modification for ZnO due to Ag doping and presence of fuel. The DRS peaks for ZnO and SZO photocatalysts are shown in Fig. 2a. The energy band gap observed for pure ZnO was 3.33 eV. All DRS spectra for Ag doped photocatalysts were made from superposition of ZnO CB peak and a visible peak due to plasmon bands formed from Ag atoms or clusters of atoms present on the surface of ZnO nanoparticles. The plasmon bands formation resulting from fluid related plasmon oscillation [49–51] was generated from clusters of Ag atoms. Thus, we expect that metal was generated during preparation process, either as cluster or as nanoparticles on the surface. This idea was favored by XPS study on the same photocatalysts. Further two more observations are worth mentioning: first is plasmon shifting to lower energy and second is increase in plasmon bands intensity as a function of increasing silver doping in ZnO. Weak plasmon band was observed at lower Ag doping but visible plasmon band was observed for 6% SZO and 8%SZO photocatalysts with peak shift from 597 nm to 532 nm possessing energy band gap of 2.07 eV and 2.33 eV respectively [52]. This confirmed the presence of Ag on ZnO surface for all Ag doped photocatalysts and increase in energy band gap intensity could be attributed to lower cluster size or smaller wavelength shift. This was a clear indication of the perpendicular orientation of dipoles connecting particles in two individual vibrations of optical excitations. Previous reports tell that charge separation is increased by metal dopants, thus improving the photocatalytic activity. The Ag doping up to 6% SZO photocatalyst resulted in a red shift of absorbance for un-doped ZnO. The energy band gap was calculated by Tauc plot

$$\alpha h\nu = [A(h\nu - Eg)]^{(1/n)}$$

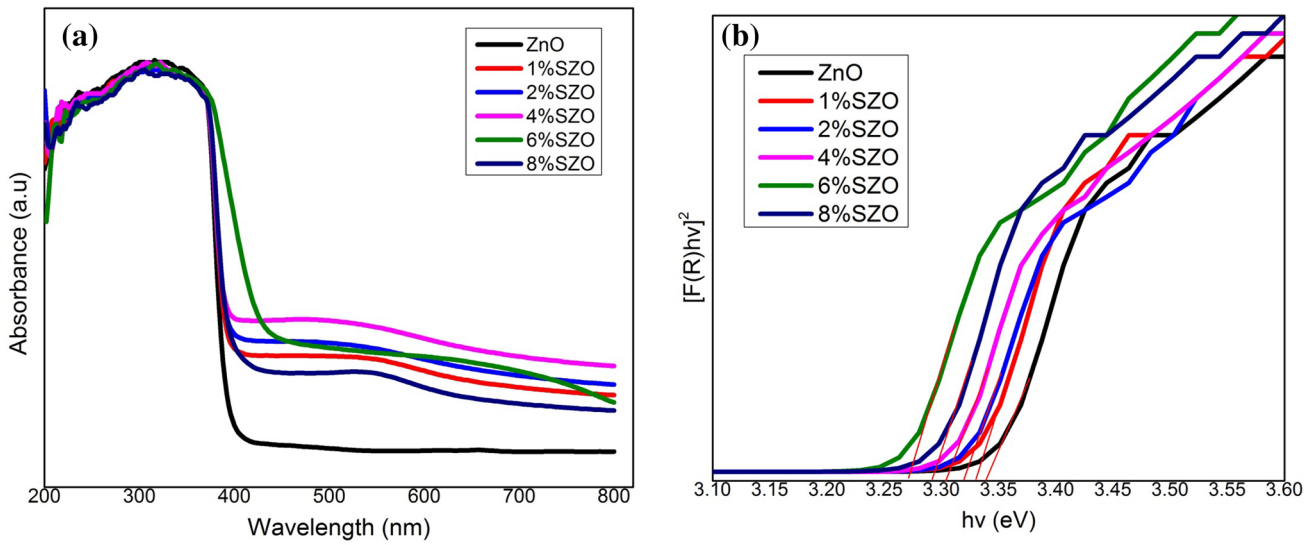

Fig. 2 Shows **a** UV–Vis DRS **b** Tauc Plot of pure ZnO and SZO photocatalysts

where A is constant, h is Planks constant, hv is energy of incident photon and Eg is energy band gap. The value of n is 1 here for direct band gap. Energy band gap (Eg) for ZnO and SZO nanoparticles was calculated by a plot between $(\alpha hv)^2$ and photon energy hv as shown in Fig. 2b. The extrapolation of the linear part of the curve to energy hv axis $(\alpha hv)^2 = 0$ estimated the energy band gap (Eg). Eg was found to be in the range of 3.27–3.33 eV as shown in Table 1.

However, energy band gap for 6% SZO photocatalyst 3.27 eV, a blue shift of 0.06 eV due to Ag doping as compared to energy band gap of pure ZnO. However it is worth mentioning that Ag doping decreased the energy band gap absorption intensity, as shown by the presence of plasmon, suppressing the penetration intensity of incoming light, perhaps due to scattering. Thus it was concluded that 6% SZO photocatalyst had the least energy band gap and will be suitable for optimal photocatalytic hydrogen evolution.

3.3 X-ray photoelectron spectroscopy

X-ray photoelectron spectroscopy (XPS) was used to examine the chemical composition, defect chemistry and physical state of silver doped ZnO (SZO) nanoparticles. The XPS spectra of Zn 2p, Ag 3d and O 1s is shown in Fig. 3. It can be observed from Fig. 3a that Zn 2p signal was divided into two symmetrical signal known as Zn $2p_{3/2}$ and Zn $2p_{1/2}$

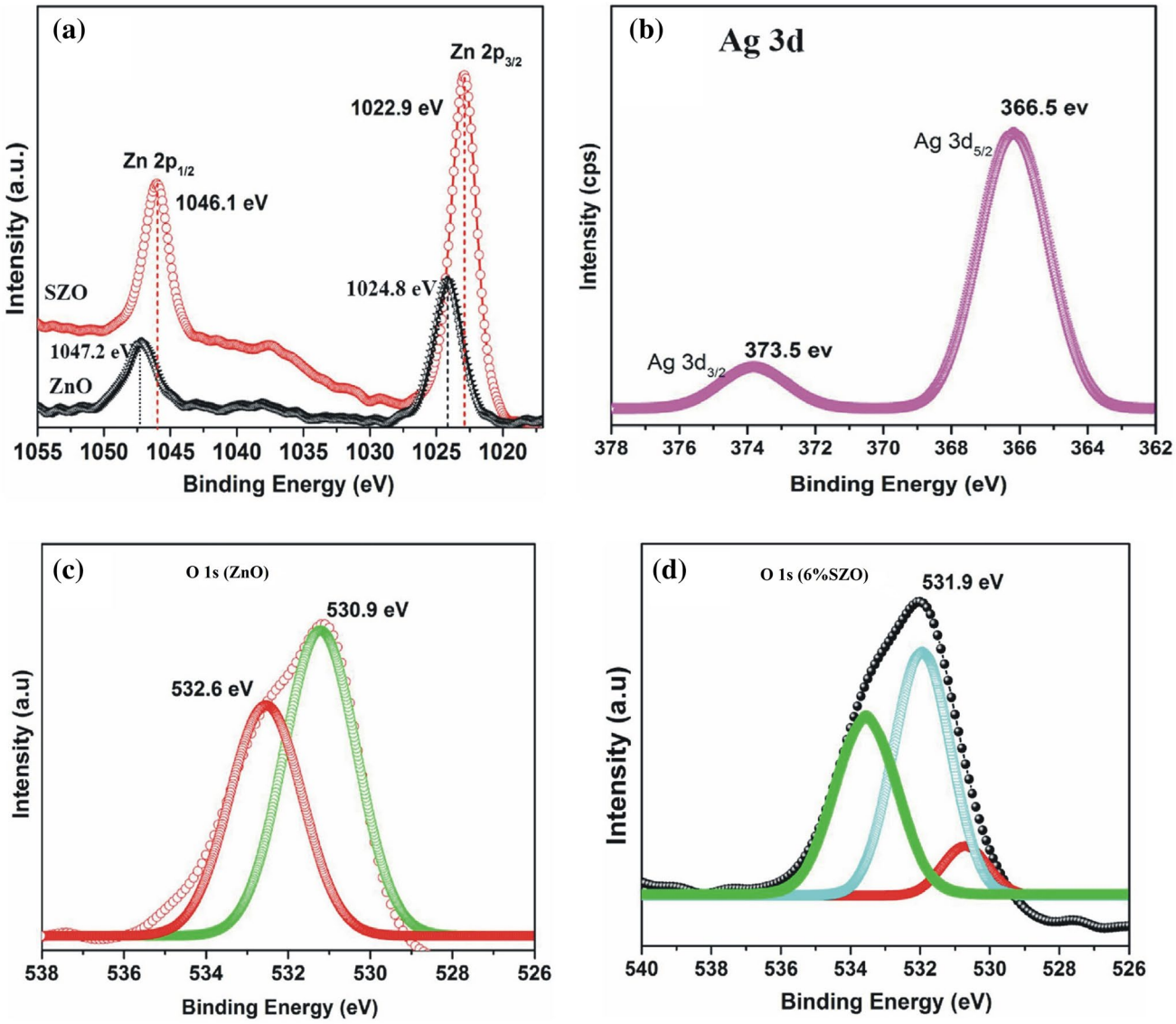

Fig. 3 Shows XPS of pure ZnO and SZO **a** Zn 2p of ZnO nanoparticles **b** Ag 2p 6% SZO **c** O 1s of ZnO nanoparticles **d** O 1s of 6% SZO photocatalyst

due to spin coupled states. These peaks were observed at 1024.8 eV and 1047.2 eV respectively for un-doped ZnO sample and peak position was slightly shifted towards smaller binding energy with Ag doping. This peak shift was due to decrease in electron density with Ag doping, the decrease in electron density resulted in enhanced binding energy. Therefore binding energy peak shifts positively, in good agreement with previous reports. Intensity is directly linked to the number of atoms in the respective chemical state. Another reason for decrease in intensity could be diffusive process. If atoms diffuse towards the surface, then an increase in intensity is observed. Higher intensity of SZO nanoparticles was due to more atoms diffused towards surface than pure ZnO [53]. The peak Zn $2p_{3/2}$ belongs to hydroxyl group linked to Zn^{+2} on the surface of ZnO nanoparticles [54], while peak Zn $2p_{1/2}$ belongs to zinc (Zn) atoms attached to oxygen (O) atoms to produce ZnO [55]. Figure 3b shows observed peaks for Ag $3d_{3/2}$ and Ag $3d_{5/2}$ at 373.5 eV and 366.5 eV respectively. Similar peaks were reported for spin orbit coupled states in previous studies [52]. Their reported peaks were observed at 373.5 eV for Ag $3d_{3/2}$ and at 367.5 eV for Ag $3d_{5/2}$ respectively, possessed spin orbit energy difference of 6 eV which was attributed to metallic silver clusters very similar to our report. Thus in our work peaks observed at 366.5 eV and 373.5 eV were due to metallic silver. Figure 3c showed O 1s signal for pure ZnO which could be deconvoluted into two peaks to explain two kinds of oxygen species. The peak observed at 530.9 eV was attributed to chemisorb as well as lattice oxygen of ZnO, while peak observed at 532.6 eV was due to presence of surface hydroxyl group [52]. Figure 3d shows O 1s spectra of 6% SZO sample which could be convoluted into three peaks located at 530.4 eV, 531.6 eV and 5.337 eV associated with O^{2-} species in the lattice (O_L), oxygen vacancies (O_V) and dissociated oxygen (O_C), respectively. The peaks were slightly shifted towards higher binding energy 531.9 eV for 6%SZO photocatalyst as compared to pure ZnO. This peak shift indicates that surface of 6% SZO was modified because of oxygen vacancies [56]. So it was concluded from XPS study that both metallic silver and silver clusters were present on the surface of ZnO nanoparticles. Thus XPS results were in agreement with both XRD and UV–Vis results.

3.4 Fourier-transform infrared spectra

Figure 4 shows FTIR spectra of ZnO and 6% SZO photocatalysts. Both photocatalysts possessed a broad absorption peak at 3442 cm^{-1} attributed to O–H bending vibration of H_2O molecule sponged on the surface of ZnO and 6% SZO samples [56]. Since photocatalytic activity is closely related to number of O–H groups because O–H group can provide an electron to photo generated hole and changed

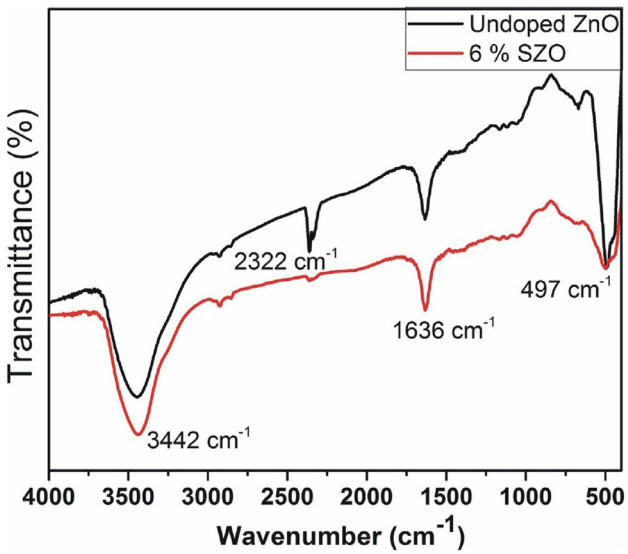

Fig. 4 Shows FTIR spectra of pure ZnO and 6% SZO photocatalyst

to reactive *OH radicals. The observed peak at 1636 cm^{-1} was attributed to bending vibration of chemisorbed H_2O on the surface of catalyst [57]. The peak observed at 2322 cm^{-1} was assigned to presence of atmospheric CO_2 in photocatalyst [58]. The peak observed at 497 cm^{-1} was produced due to stretched vibrations of Zn–O bond [59]. Thus FTIR was used to observe the influence of Ag loading and showed no evidence for formation of AgO or Ag_2O bands [60]. Thus formation of Ag should be in metallic silver and further there was neither observed new chemical bond nor bond between Ag–O and Ag–ZnO. These results were in agreement with XRD results on Ag doping in ZnO lattice, Ag doping formed metallic silver cluster.

3.5 Photoluminescence spectra

Photoluminescence spectroscopy (PL) is a good technique to study the crystal quality and existence of impurities in catalyst. Generally, photoluminescence spectra of ZnO nanoparticles consist of ultraviolet (UV) and visible emission band. UV emission is assigned to exciton recombination rate [61] and might be called band gap emission. Structural defects and/or surface impurities are responsible for visible emission broadband [62]. Figure 5 shows room temperature PL spectra of synthesized pure ZnO and SZO photocatalysts. A strong UV emission around 391 nm and several peaks with small emission for visible broad band were observed for unloaded ZnO sample. The PL emission at 460 nm was due to radiative transition of an electron from the shallow donor level of Zn interstitial (Zn_i) to acceptor level of neutral V_{Zn}. This emission might be related to surface defects of ZnO nanoparticles or may be due to singly ionized V_{Zn}

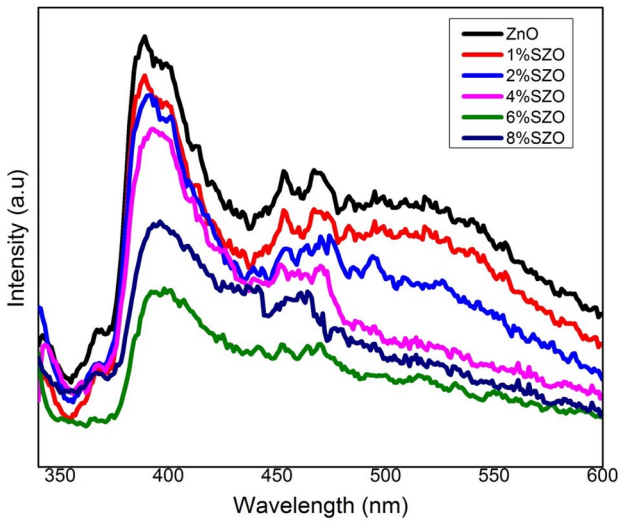

Fig. 5 PL spectra of pure ZnO and SZO photocatalysts

although the detailed mechanism for blue emission at 460 nm has not been clarified. Also with increase in Ag doping, both UV and broadband visible emission intensity were reduced for SZO photocatalysts with broadening and shifting of PL emission intensity towards larger wavelength. Ag doped ZnO nanoparticles had shown very small luminescence as compared to pure ZnO nanoparticles [62]. The lowest PL emission intensity of 6% SZO photocatalyst revealed that electron hole pair rate is greatly suppressed and will be suitable to show optimal photocatalytic hydrogen evolution. PL emission spectra showed that Ag doped ZnO photocatalyst did not show presence of new emission band at room temperature, in good agreement to earlier observations [62].

3.6 BET surface area

Brunauer–Emmett Teller (BET) surface area showed very small variation in surface area on Ag doping. The observed increased surface area with Ag doping revealed that Ag was producing legroom into ZnO nano crystals. The BET surface area increased obviously to 31 $m^2\ g^{-1}$ after 8% Ag doping into ZnO. The results are shown in Table 1. The doping of Ag suppressed the growth of ZnO phase noticeably, resulted in a small increase in BET surface area, retain porosity and generated shallow type new pores. The retarded growth of ZnO may be attributed to combustion synthesis, which was a rapid method in which the product was synthesized with a few minutes at high temperature; the presence of Ag retarded the growth of ZnO. The slight increase in surface area for Ag doped ZnO photocatalyst was attributed to decrease in particle size with Ag doping.

3.7 Scanning electron microscopy

Surface morphology, crystal size, crystal shape and growth mechanism of synthesized pure ZnO and Ag loaded ZnO nanoparticles were studied by SEM. It can be observed from Fig. 6 that particles are closely packed, nearly spherical in shape and randomly oriented. The non-uniform distribution of silver nanoparticles on ZnO nanostructure can be attributed to site selection position of Ag on ZnO. Hence silver nanoparticles could produce metallic clusters or tend to generate nanoparticles agglomeration at different sites of ZnO nanoparticles, the generation of metallic clusters or large agglomeration was supported by XRD (111) and (200) metallic Ag peaks. It was also supported by UV–Vis study due to presence of surface plasmon bands and XPS study by clusters formation. The particle size measured for pure ZnO sample was 18 nm and reduced for SZO samples with Ag doping, complemented by XRD results and BET surface area. Thus it was concluded that formation of metallic clusters become strong with Ag doping due to which photocatalytic activity will enhance since clusters were efficient to trap electrons.

3.8 EDX analysis

EDX spectra were used to study the elemental composition of the synthesized pure ZnO and Ag doped ZnO samples. The EDX spectra of pure ZnO and 6%SZO samples are shown in Fig. 7. EDX spectra of pure ZnO contained only Zn and O elements, while EDX spectra of 6%SZO catalyst revealed the presence of Ag in addition to Zn and O elements.

3.9 I–V measurement

Figure 8 shows I–V measurements for ZnO and SZO nanoparticles. It can be observed from figure that resistivity was decreased with increase in silver concentration. The resistivity of the SZO nanoparticles was lower than that of pure ZnO nanoparticles due to creation of more charge carriers with silver doping. The resistivity was reduced due to an increase in the free-electron concentration with silver incorporation in the ZnO lattice [65].

4 Photocatalytic hydrogen evolutions

The synthesized ZnO and SZO photocatalysts were tested for hydrogen evolution from water ethanol solution. Ethanol was used as sacrificial agent due to its good previous record. There exists some appropriate quantity of ethanol for optimal hydrogen evolution. Water was reduced to H_2 by photo generated electron transition to conduction

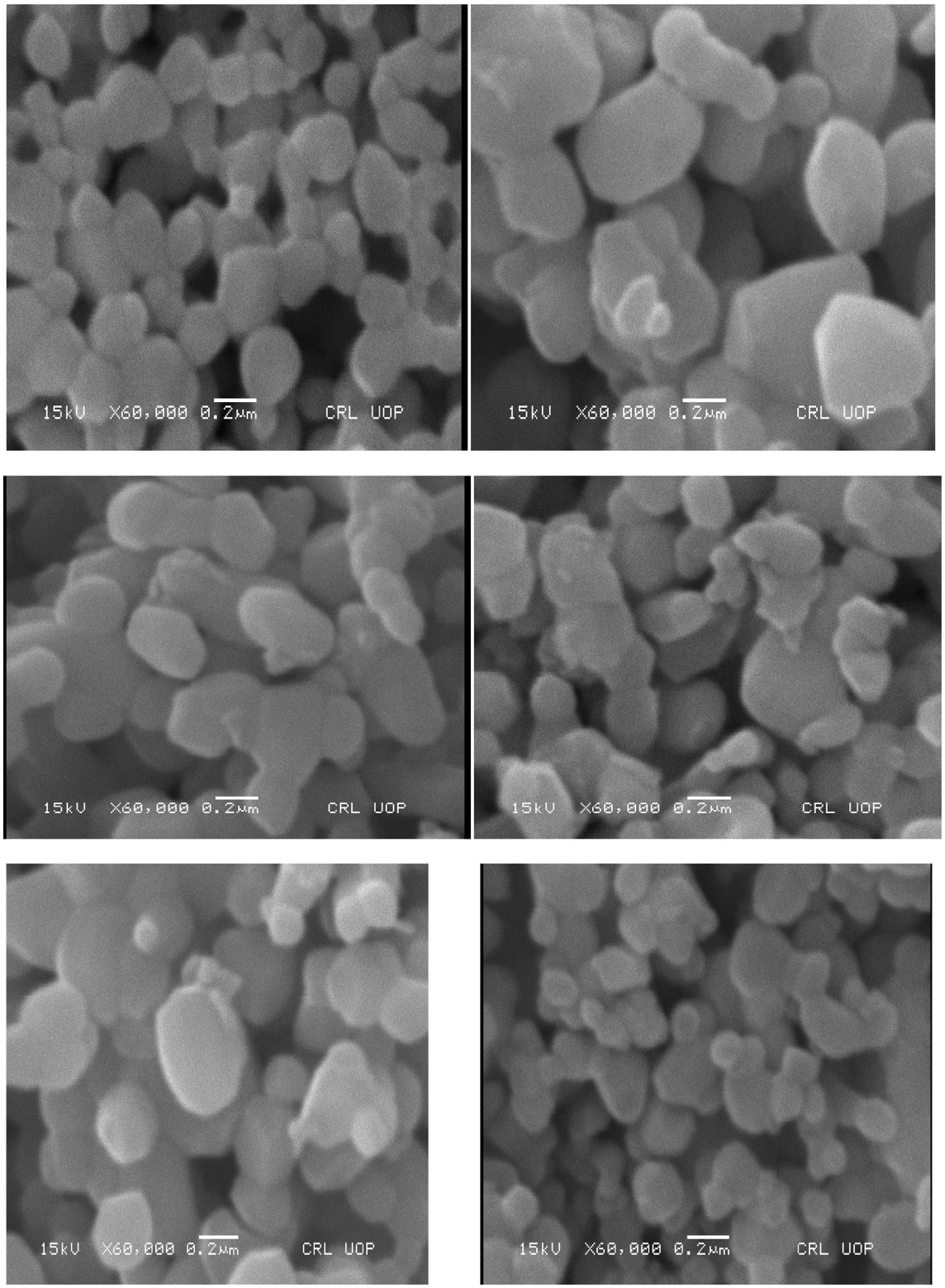

Fig. 6 Exhibits SEM images of ZnO, 1%SZO, 2%SZO, 4%SZO, 6%SZO and 8%SZO respectively

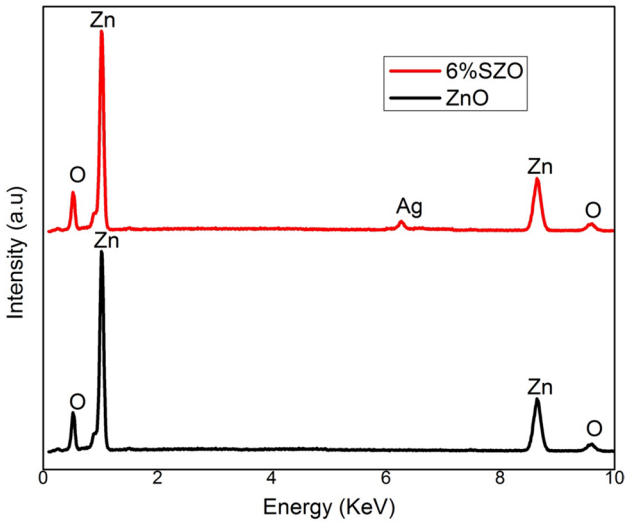

Fig. 7 Exhibits EDX spectra of ZnO and 6%SZO

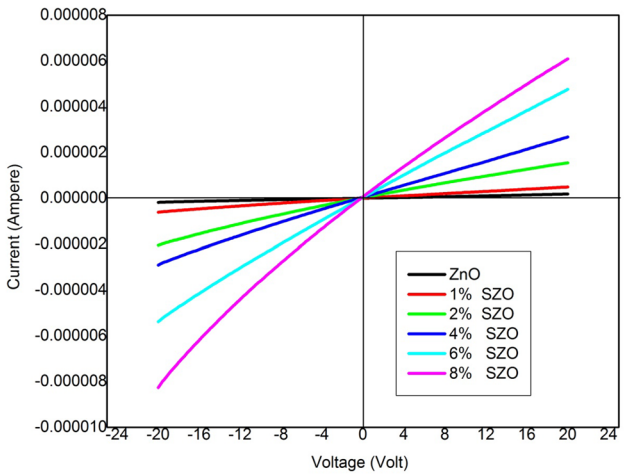

Fig. 8 Exhibits I–V measurements of pure ZnO and 6% SZO photocatalyst

band (CB) accompanied by oxidation of ethanol. Acetaldehyde would be formed due to interaction between ethanol and surface trapped holes.

$$2h^+ + C_2H_5OH \rightarrow 2H^+ + CH_3CHO \quad (1)$$

Further, acetic acid would result from oxidation of acetaldehyde

$$2h^+ + CH_3CHO \rightarrow 2H^+ + CH_3COOH \quad (2)$$

The photo generated electron in CB reduces H^+ to generate H_2 while CH_3COOH decompose into CO_2 and CH_4 as shown in Fig. 9. Similar photocatalytic hydrogen evolution activity from ethanol water solution was reported [1]. It was observed that hydrogen evolution

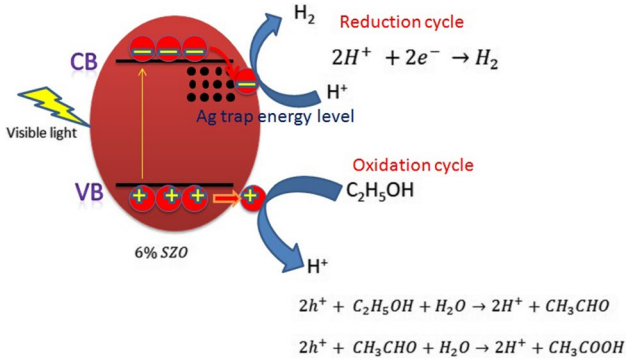

Fig. 9 Exhibit schematic diagram for purposed photocatalytic mechanism for hydrogen evolution over 6% SZO photocatalyst under visible light irradiation

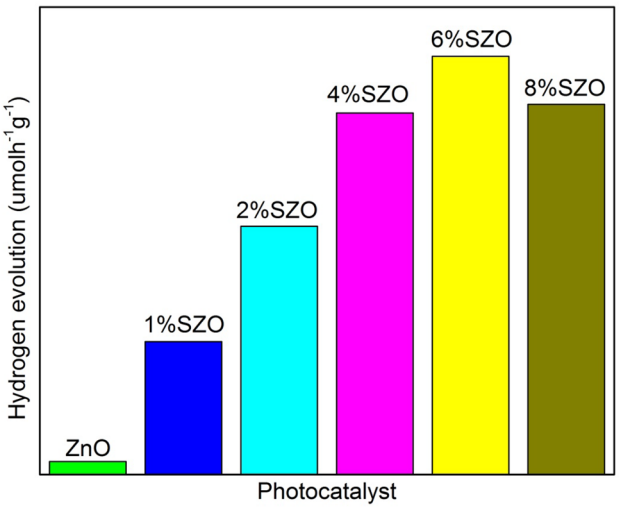

Fig. 10 Shows hydrogen evolution rate for pure ZnO and SZO photocatalysts

rate was enhanced with increasing catalyst amount. It is acceptable because increasing Ag–ZnO quantity would generate more active centers due to increase in surface area and increase in H_2 generation rate. Generally, hydrogen evolution rate is enhanced with increase in catalyst amount due to increase in active sites of photocatalyst. However beyond some photocatalyst quantity, hydrogen evolution rate was decreased because surface area would decrease due to aggregation of the photocatalysts [1]. Similar result was observed in our work for 8% SZO photocatalyst whose H_2 evolution rate was decreased as compared to 6% SZO photocatalyst. This decreased H_2 evolution rate could be attributed to light scattering and retardation of light penetration through ZnO [63]. It can be observed form Fig. 10 that pure ZnO showed minimum hydrogen evolution rate of 15 µmol h^{-1} g^{-1}, which was attributed to its wide band

gap (3.20 eV) and absence of hydrogen generation sites on the ZnO surface. The loading of Ag slightly shifted the absorption band edge of ZnO into visible range [64]. The Ag doping into ZnO modified energy levels so that electron could be easily excited from valence band (VB) to CB of ZnO, which reduced water to H_2. Ag doping could be responsible for two reasons in photocatalyst process. Firstly, doping sites may act as trapping pool for charge carriers, which would be useful for charge separation and improved photocatalytic activity. Secondly, it may exist as crystal defects which would act as recombination centers for photo produced charges (electrons, holes) as mostly loaded ions act as accommodation sites to capture electrons while higher loading concentration could result in generation of more defects [64]. The hydrogen evolution rate for ZnO and SZO photocatalyst is shown in Table 1. It was observed that 6% SZO photocatalyst showed optimal hydrogen evolution rate of 805 μmol h^{-1} g^{-1}. Further increase in Ag content; resulted in reduction of H_2 evolution rate. It might be attributed to retarded light absorption ability and increased recombination centers. The higher Ag doped ZnO may retarded light absorption ability of ZnO and may transport undesired charge carriers due to presence of phase boundary. Thus hydrogen evolution rate was initially increased as a function of Ag doping and photocatalyst content and reduced at higher Ag doping as shown in Fig. 9.

5 Conclusion

In this paper synthesis of ZnO and Ag doped ZnO nanoparticles using combustion method and their photocatalytic activity for hydrogen evolution have been studied. The impact of various Ag doping contents on ZnO was investigated by XRD, DRS, PL, XPS, FTIR, SEM, BET surface area and EDX analysis. It can be found that content of Ag has a optimal value, which can suppress the electron hole pair recombination so as to increase the photocatalytic activity. The absorption edge of SZO nanoparticles in UV–Vis absorbance spectra had a pronounced red shift. High content of silver (8%SZO) can become the recombination centre for electrons and holes and is the cause of decreased photocatalytic activity. Hydrogen evolution rate of 6%SZO catalyst was increased to 805 μmol h^{-1} g^{-1} which was approximately 54 times greater than to pure ZnO due to the excellent effects of silver doping. Thus present results indicate that SZO photocatalysts are potential candidate for future practical for hydrogen evolution by water splitting.

Compliance with ethical standards

Conflict of interest Authors declare that there are no conflict of interest statements.

References

1. Bang KH, Hwang DK, Myoung JM (2003) Effects of ZnO buffer layer thickness on properties of ZnO thin films deposited by radio-frequency magnetron sputtering. Appl Surf Sci 207(1–4):359–364. https://doi.org/10.1016/S0169-4332(03)00005-9
2. Yan Z, Song ZT, Liu WL, Wan Q, Zhang FM, Feng SL (2005) Optical and electrical properties of p-type zinc oxide thin films synthesized by ion beam assisted deposition. Thin Solid Films 492(1–2):203–206. https://doi.org/10.1016/j.tsf.2005.06.035
3. Broasca G, Borcia G, Dumitrascu N, Vrinceanu N (2013) Characterization of ZnO coated polyester fabrics for UV protection. Appl Surf Sci 279:272–278. https://doi.org/10.1016/j.apsusc.2013.04.084
4. Abdi Y, Khadem SJ, Afzali P (2014) Resonantly excited ZnO nanowires for fabrication of high sensitivity gas sensor. Curr Appl Phys 14(3):227–231. https://doi.org/10.1016/j.cap.2013.11.020
5. Klingshirn C (2007) ZnO: from basics towards applications. Phys Status Solidi (b) 244(9):3027–3073. https://doi.org/10.1002/pssb.200743072
6. Fortunato E, Pereira L, Barquinha P, Ferreira I, Prabakaran R, Goncalves G, Goncalves A, Martins R (2009) Oxide semiconductors: order within the disorder. Phil Mag 89(28–30):2741–2758. https://doi.org/10.1080/14786430903022671
7. Park SY, Kim BJ, Kim K, Kang MS, Lim KH, Lee TI, Myoung JM, Baik HK, Cho JH, Kim YS (2012) Low-temperature, solution-processed and alkali metal doped ZnO for high-performance thin-film transistors. Adv Mater 24(6):834–838. https://doi.org/10.1002/adma.201103173
8. Ebothe J, Kityk IV, Benet S, Claudet B, Plucinski KJ, Ozga K (2006) Photoinduced effects in ZnO films deposited on MgO substrates. Opt Commun 268(2):269–272. https://doi.org/10.1016/j.optcom.2006.07.017
9. Hu P, Han N, Zhang D, Ho JC, Chen Y (2012) Highly formaldehyde-sensitive, transition-metal doped ZnO nanorods prepared by plasma-enhanced chemical vapor deposition. Sens Actuators B Chem 169:74–80. https://doi.org/10.1016/j.snb.2012.03.035
10. Bougrine A, El Hichou A, Addou M, Ebothé J, Kachouane A, Troyon M (2003) Structural, optical and cathodoluminescence characteristics of undoped and tin-doped ZnO thin films prepared by spray pyrolysis. Mater Chem Phys 80(2):438–445. https://doi.org/10.1016/s0254-0584(02)00505-9
11. Wu Y, Girgis E, Ström V, Voit W, Belova L, Rao KV (2011) Ultraviolet light sensitive In-doped ZnO thin film field effect transistor printed by inkjet technique. Phys Status Solidi (a) 208(1):206–209
12. Mahdhi H, Ben Ayadi Z, El Mir L, Djessas K, Alaya S (2011) Elaboration and characterization of Ca doped ZnO films prepared by rf-magnetron sputtering at room temperature. Sens Lett 9(6):2150–2153. https://doi.org/10.1166/sl.2011.1758
13. Ayadi ZB, El Mir L, Djessas K, Alaya S (2007) Electrical and optical properties of aluminum-doped zinc oxide sputtered from an aerogel nanopowder target. Nanotechnology 18(44):445702. https://doi.org/10.1088/0957-4484/18/44/445702
14. Ben Ayadi Z, El Mir L, Djessas K, Alaya S (2009) Transparent and conductive aluminum doped zinc oxide films sputtered

from aerogel nanopowders. Sens Lett 7(5):702–706. https://doi.org/10.1166/sl.2009.1134
15. Ahmad M, Ahmed E, Zhang Y, Khalid NR, Xu J, Ullah M, Hong Z (2013) Preparation of highly efficient Al-doped ZnO photocatalyst by combustion synthesis. Curr Appl Phys 13(4):697–704. https://doi.org/10.1016/j.cap.2012.11.008
16. Cheng B, Xiao Y, Wu G, Zhang L (2004) The vibrational properties of one-dimensional ZnO: Ce nanostructures. Appl Phys Lett 84(3):416–418. https://doi.org/10.1063/1.1639131
17. Kanemitsu Y, Suzuki K, Nakayoshi Y, Masumoto Y (1992) Quantum size effects and enhancement of the oscillator strength of excitons in chains of silicon atoms. Phys Rev B 46(7):3916. https://doi.org/10.1103/physrevb.46.3916
18. Karthikeyan B, Sandeep CS, Philip R, Baesso ML (2009) Study of optical properties and effective three-photon absorption in Bi-doped ZnO nanoparticles. J Appl Phys 106(11):114304. https://doi.org/10.1063/1.3259404
19. Akyol A, Yatmaz HC, Bayramoglu M (2004) Photocatalytic decolorization of Remazol Red RR in aqueous ZnO suspensions. Appl Catal B 54(1):19–24. https://doi.org/10.1016/j.apcatb.2004.05.021
20. Kavitha R, Meghani S, Jayaram V (2007) Synthesis of titania films by combustion flame spray pyrolysis technique and its characterization for photocatalysis. Mater Sci Eng B 139(2–3):134–140. https://doi.org/10.1016/j.mseb.2007.01.040
21. Mahdhi H, Ayadi ZB, Gauffier JL, Djessas K, Alaya S (2015) Effect of sputtering power on the electrical and optical properties of Ca-doped ZnO thin films sputtered from nanopowders compacted target. Opt Mater 45:97–103. https://doi.org/10.1016/j.optmat.2015.03.015
22. Schroder DK (2006) Semiconductor material and device characterization. Wiley, Hoboken
23. Pankove J (1976) Optical processes in semiconductors (Do-ver, New York, 1971). C. Kittel, Introduction to solid state physics, p 289. https://trove.nla.gov.au/version/45414559. Accessed 27 Aug 2018
24. Ayadi ZB, El Mir L, Djessas K, Alaya S (2011) Effect of substrate temperature on the properties of Al-doped ZnO films sputtered from aerogel nanopowders for solar cells applications. Thin Solid Films 519(21):7572–7574. https://doi.org/10.1016/j.tsf.2010.12.120
25. Pejova B (2010) The Urbach–Martienssen absorption tails in the optical spectra of semiconducting variable-sized zinc selenide and cadmium selenide quantum dots in thin film form. Mater Chem Phys 119(3):367–376. https://doi.org/10.1016/j.matchemphys.2009.08.064
26. Shimizu T (1978) Chemical trends for localized gap states in amorphous semiconductors. Solid State Commun 25(7):455–456. https://doi.org/10.1016/0038-1098(78)90155-2
27. Matthews RW (1989) Photocatalytic oxidation and adsorption of methylene blue on thin films of near-ultraviolet-illuminated TiO_2. J Chem Soc Faraday Trans 1 Phys Chem Condens Phases 85(6):1291–1302. https://doi.org/10.1039/f19898501291
28. Elsellami L, Vocanson F, Dappozze F, Baudot R, Febvay G, Rey M, Houas A, Guillard C (2010) Kinetics and initial photocatalytic pathway of tryptophan, important constituent of microorganisms. Appl Catal B 94(1–2):192–199. https://doi.org/10.1016/j.apcatb.2009.11.009
29. Helali S, Puzenat E, Perol N, Safi MJ, Guillard C (2011) Methylamine and dimethylamine photocatalytic degradation—adsorption isotherms and kinetics. Appl Catal A 402(1–2):201–207. https://doi.org/10.1016/j.apcata.2011.06.004
30. Rauf MA, Meetani MA, Hisaindee S (2011) An overview on the photocatalytic degradation of azo dyes in the presence of TiO_2 doped with selective transition metals. Desalination 276(1–3):13–27. https://doi.org/10.1016/j.desal.2011.03.071
31. Herrmann JM (2010) Photocatalysis fundamentals revisited to avoid several misconceptions. Appl Catal B 99(3–4):461–468. https://doi.org/10.1016/j.apcatb.2010.05.012
32. Sauer T, Neto GC, Jose HJ, Moreira RFPM (2002) Kinetics of photocatalytic degradation of reactive dyes in a TiO_2 slurry reactor. J Photochem Photobiol A 149(1–3):147–154. https://doi.org/10.1016/S1010-6030(02)00015-1
33. Karthikeyan B, Pandiyarajan T, Mangaiyarkarasi K (2011) Optical properties of sol–gel synthesized calcium doped ZnO nanostructures. Spectrochim Acta A Mol Biomol Spectrosc 82(1):97–101. https://doi.org/10.1016/j.saa.2011.07.005
34. Slama R, El Ghoul J, Omri K, Houas A, El Mir L, Launay F (2016) Effect of Ca-doping on microstructure and photocatalytic activity of ZnO nanoparticles synthesized by sol gel method. J Mater Sci Mater Electron 27(8):7939–7946. https://doi.org/10.1007/s10854-016-4786-9
35. Kolesnik S, Dabrowski B, Mais J (2004) Structural and magnetic properties of transition metal substituted ZnO. J Appl Phys 95(5):2582–2586. https://doi.org/10.1063/1.1644638
36. Herng TS, Lau SP, Yu SF, Yang HY, Ji XH, Chen JS, Yasui N, Inaba H (2006) Origin of room temperature ferromagnetism in ZnO: Cu films. J Appl Phys. https://doi.org/10.1063/1.2190711
37. Saeki H, Tabata H, Kawai T (2001) Magnetic and electric properties of vanadium doped ZnO films. Solid State Commun 120(11):439–443. https://doi.org/10.1016/S0038-1098(01)00400-8
38. Ramachandran S, Tiwari A, Narayan J, Prater JT (2005) Epitaxial growth and properties of $Zn_{1-x}V_xO$ diluted magnetic semiconductor thin films. Appl Phys Lett 87(17):172502. https://doi.org/10.1063/1.2112185
39. Wang JD, Liu JK, Tong Q, Lu Y, Yang XH (2014) High degradation activity and quantity production of aluminum-doped zinc oxide nanocrystals modified by nitrogen atoms. Ind Eng Chem Res 53(6):2229–2237. https://doi.org/10.1007/s10854-016-4786-9
40. Huo J, Fang L, Lei Y, Zeng G, Zeng H (2014) Facile preparation of yttrium and aluminum co-doped ZnO via a sol–gel route for photocatalytic hydrogen production. J Mater Chem A 2(29):11040–11044. https://doi.org/10.1039/c4ta02207f
41. Chen PK, Lee GJ, Anandan S, Wu JJ (2012) Synthesis of ZnO and Au tethered ZnO pyramid-like microflower for photocatalytic degradation of orange II. Mater Sci Eng B 177(2):190–196. https://doi.org/10.1021/ic700688f
42. Xu J, Pan Q, Tian Z (2000) Grain size control and gas sensing properties of ZnO gas sensor. Sens Actuators B Chem 66(1–3):277–279. https://doi.org/10.1016/S0925-4005(99)00422-0
43. Mimouni R, Souissi A, Madouri A, Boubaker K, Amlouk M (2017) High photocatalytic efficiency and stability of chromium-indium codoped ZnO thin films under sunlight irradiation for water purification development purposes. Curr Appl Phys 17(8):1058–1065. https://doi.org/10.1016/j.vacuum.2018.05.051
44. Usai S, Obregón S, Becerro AI, Colón G (2013) Monoclinic–tetragonal heterostructured $BiVO_4$ by yttrium doping with improved photocatalytic activity. J Phys Chem C 117(46):24479–24484. https://doi.org/10.1021/jp409170y
45. Gao P, Liu Z, Sun DD (2013) The synergetic effect of sulfonated graphene and silver as co-catalysts for highly efficient photocatalytic hydrogen production of ZnO nanorods. J Mater Chem A 1(45):14262–14269. https://doi.org/10.1039/c3ta13047a
46. Martha S, Reddy KH, Parida KM (2014) Fabrication of In 2 O 3 modified ZnO for enhancing stability, optical behaviour, electronic properties and photocatalytic activity for hydrogen production under visible light. J Mater Chem A 2(10):3621–3631. https://doi.org/10.1039/c3ta14285j
47. Su CY, Lu CT, Hsiao WT, Liu WH, Shieu F (2013) Evaluation of the microstructural and photocatalytic properties of aluminum-doped zinc oxide coatings deposited by

plasma spraying. Thin Solid Films 544:170–174. https://doi.org/10.1016/j.tsf.2013.03.129
48. Zhan Z, Wang Y, Lin Z, Zhang J, Huang F (2011) Study of interface electric field affecting the photocatalysis of ZnO. Chem Commun 47(15):4517–4519. https://doi.org/10.1039/c1cc10888c
49. Hamden Z, Ferreira DP, Ferreira LV, Bouattour S (2014) Li–Y doped and codoped TiO_2 thin films: enhancement of photocatalytic activity under visible light irradiation. Ceram Int 40(2):3227–3235. https://doi.org/10.1016/j.ceramint.2013.09.114
50. Kochuveedu ST, Jang YH, Jang YJ, Kim DH (2013) Visible light active photocatalysis on block copolymer induced strings of ZnO nanoparticles doped with carbon. J Mater Chem A 1(3):898–905. https://doi.org/10.1039/c2ta00263a
51. Martha S, Reddy KH, Parida KM (2014) Fabrication of In 2 O 3 modified ZnO for enhancing stability, optical behaviour, electronic properties and photocatalytic activity for hydrogen production under visible light. J Mater Chem A 2(10):3621–3631. https://doi.org/10.1039/c3ta14285j
52. Freire PG, Montes RH, Romeiro FC, Lemos SC, Lima RC, Richter EM, Munoz RA (2016) Morphology of ZnO nanoparticles bound to carbon nanotubes affects electrocatalytic oxidation of phenolic compounds. Sens Actuators B Chem 223:557–565. https://doi.org/10.1016/j.snb.2015.09.086
53. Krishnakumar B, Subash B, Swaminathan M (2012) AgBr–ZnO–An efficient nano-photocatalyst for the mineralization of Acid Black 1 with UV light. Sep Purif Technol 85:35–44. https://doi.org/10.1016/j.seppur.2011.09.037
54. Nada AA, Barakat MH, Hamed HA, Mohamed NR, Veziroglu TN (2005) Studies on the photocatalytic hydrogen production using suspended modified TiO_2 photocatalysts. Int J Hydrogen Energy 30(7):687–691. https://doi.org/10.1016/j.ijhydene.2004.06.007
55. Ni M, Leung MK, Leung DY, Sumathy K (2007) A review and recent developments in photocatalytic water-splitting using TiO_2 for hydrogen production. Renew Sustain Energy Rev 11(3):401–425. https://doi.org/10.1016/j.rser.2005.01.009
56. Tam KH, Cheung CK, Leung YH, Djurišić AB, Ling CC, Beling CD, Fung S, Kwok WM, Chan WK, Phillips DL, Ding L (2006) Defects in ZnO nanorods prepared by a hydrothermal method. J Phys Chem B 110(42):20865–20871. https://doi.org/10.1021/jp063239w
57. Galińska A, Walendziewski J (2005) Photocatalytic water splitting over Pt–TiO_2 in the presence of sacrificial reagents. Energy Fuels 19(3):1143–1147. https://doi.org/10.1021/ef0400619
58. Amirav L, Alivisatos AP (2010) Photocatalytic hydrogen production with tunable nanorod heterostructures. J Phys Chem Lett 1(7):1051–1054. https://doi.org/10.1021/jz100075c
59. Kim S, Choi W (2002) Dual photocatalytic pathways of trichloroacetate degradation on TiO_2: effects of nanosized platinum deposits on kinetics and mechanism. J Phys Chem B 106(51):13311–13317. https://doi.org/10.1021/jp0262261
60. Yi H, Peng T, Ke D, Ke D, Zan L, Yan C (2008) Photocatalytic H_2 production from methanol aqueous solution over titania nanoparticles with mesostructures. Int J Hydrogen Energy 33(2):672–678. https://doi.org/10.1038/srep13475
61. Huang BS, Chang FY, Wey MY (2010) Photocatalytic properties of redox-treated Pt/TiO_2 photocatalysts for H_2 production from an aqueous methanol solution. Int J Hydrogen Energy 35(15):7699–7705. https://doi.org/10.1016/j.ijhydene.2010.05.103
62. Choi HJ, Kang M (2007) Hydrogen production from methanol/water decomposition in a liquid photosystem using the anatase structure of Cu loaded TiO_2. Int J Hydrogen Energy 32(16):3841–3848. https://doi.org/10.1016/j.ijhydene.2007.05.011
63. Huo J, Fang L, Lei Y, Zeng G, Zeng H (2014) Facile preparation of yttrium and aluminum co-doped ZnO via a sol–gel route for photocatalytic hydrogen production. J Mater Chem A 2(29):11040–11044. https://doi.org/10.1039/c4ta02207f
64. Zhan Z, Wang Y, Lin Z, Zhang J, Huang F (2011) Study of interface electric field affecting the photocatalysis of ZnO. Chem Commun 47(15):4517–4519. https://doi.org/10.1039/c1cc10888c
65. Sahal M, Hartiti B, Ridah A, Mollar M, Mari B (2008) Structural, electrical and optical properties of ZnO thin films deposited by sol–gel method. Microelectron J 39(12):1425–1428. https://doi.org/10.1016/j.mejo.2008.06.085

Publisher's Note Springer Nature remains neutral with regard to jurisdictional claims in published maps and institutional affiliations.